Photoactivatable Fluorophores for Bioimaging Applications

Yang Zhang,§,* Yeting Zheng,¶ Andrea Tomassini,¶ Ambarish Kumar Singh,¶ and Françisco M. Raymo¶,*

- § Program of Polymer and Color Chemistry, Department of Textile Engineering, Chemistry and Science, North Carolina State University, Raleigh, NC 27606
- Laboratory for Molecular Photonics, Department of Chemistry, 1301 Memorial Drive, University of Miami, Coral Gables, FL 33146-0431

ABSTRACT: Photoactivatable fluorophores provide the opportunity to switch fluorescence on exclusively in a selected area within a sample of interest at a precise interval of time. Such a level of spatiotemporal fluorescence control enables the implementation of imaging schemes to monitor dynamic events in real time and visualize structural features with nanometer resolution. These transformative imaging methods are contributing fundamental insights on diverse cellular processes with profound implications in biology and medicine. Current photoactivatable fluorophores, however, become emissive only after the activation event, preventing the acquisition of fluorescence images and, hence, the visualization of the sample prior to activation. We developed a family of photoactivatable fluorophores capable of interconverting between emissive states with spectrally-resolved fluorescence, instead of switching from a nonemissive state to an emissive one. We demonstrated that our compounds allow the real-time monitoring of molecules diffusing across the cellular blastoderm of developing embryos as well as of polymer beads translocating along the intestinal tract of live nematodes. Additionally, they also permit the tracking of single molecules in the lysosomal compartments of live cells and the visualization of these organelles with nanometer resolution. Indeed, our photoactivatable fluorophores may evolve into invaluable analytical tools for the investigation of the fundamental factors regulating the functions and structures of cells at the molecular level.

KEYWORDS: fluorescence photoactivation and dissipation (FPD), photoactivatable fluorophores (PAFs), photoactivated localization microscopy (PALM), photochemical barcoding, single-molecule localization microscopy (SMLM), single-particle tracking photoactivated localization microscopy (spt-PALM)

1. INTRODUCTION

Conventional fluorophores produce fluorescence upon irradiation at an appropriate excitation wavelength (λ_{Ex}) . Photoactivatable fluorophores, instead, emit significantly only if illumination at λ_{Ex} follows irradiation at a suitable activation wavelength (λ_{Ac}) . Indeed, absorption of radiation at λ_{Ac} initiates the photochemical conversion of a nonemissive reactant into an emissive product, which is then excited at λ_{Ex} to generate fluorescence.

Two alternative mechanisms can be invoked to photoactivate fluorescence. One controls the relaxation dynamics of the first singlet excited state (S_1) . The other regulates the absorption characteristics of the ground state (S_0) . Both demand the covalent integration of a photocleavable protecting group and a fluorescent chromophore (photocage and fluorophore in Figure 1) in the same molecular construct. Irradiation at λ_{Ac} cleaves the photocage from the fluorophore and, if one component can diffuse away from the other, encourages their physical separation. This photochemical step can be engineered to enhance the fluorescence quantum yield of the fluorophore $(S_1 \text{ control})$ or shift bathochromically its absorption $(S_0 \text{ control})$.

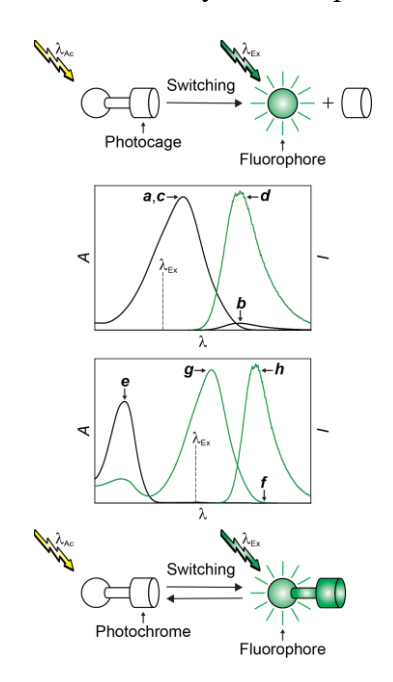


Figure 1. Irreversible and reversible fluorescence photoactivation in photocage—fluorophore and photochrome—fluorophore constructs respectively together with schematic representations of the absorption and emission spectra before (black) and after (green) switching for photoactivation mechanisms based on S_1 (a–d) and S_0 (e–h) control.

In photoactivatable fluorophores based on S_1 control, the photocage is designed to quench intramolecularly the excited fluorophore as a result of electron or energy transfer.^{6,8} Under these conditions, excitation at a λ_{Ex} within the absorption band of the fluorophore (\boldsymbol{a} in Figure 1) produces negligible fluorescence (\boldsymbol{b} in Figure 1) prior to activation. After activation, the photocage diffuses away from the fluorophore and excitation at the very same λ_{Ex} (\boldsymbol{c} in Figure 1) generates intense fluorescence (\boldsymbol{d} in Figure 1). Unitary quenching efficiencies in the initial state, however, are not accessible in most instances. Hence, the emission intensity of photoactivatable fluorophores, based on S_1 control, can only switch from low to high values, rather than from fully off to on. As a result, the ratio (contrast) between the emission intensity after and that before switching is often modest. The other significant disadvantage of this photoactivation mechanism is that the absorption properties of the fluorophore do not change significantly with switching (\boldsymbol{a} and \boldsymbol{c} in Figure 1), preventing the possibility to excite selectively the photochemical product in the presence of the reactant.

In photoactivatable fluorophores based on S_0 control, the photoinduced cleavage of the photocage from the fluorophore is designed to extend electronic delocalization within the latter component.^{6,8} Such a change in electronic structure shifts the absorption band of the fluorophore bathochromically (e and g in Figure 1) to enable the selective excitation of the photochemical product. Under illumination a λ_{Ex} positioned within the shifted absorption band, significant fluorescence is, indeed, detected only after the photochemical transformation (f and h in Figure 1). As a result, this photoactivation mechanism provides access to infinite contrast.

The photoinduced cleavage of the photocage from the fluorophore is irreversible. 6,8 It follows that the photoactivated fluorescence cannot be turned back off, irrespectively of the switching mechanism, unless the emissive product is intentionally bleached. Alternatively, the photocage can be replaced with a photochromic component (photochrome in Figure 1) to enable the reversible switching of fluorescence. Indeed, photochromic compounds switch reversibly between two states with distinct absorption properties. 19 One of the two interconvertible states of the photochrome can be engineered to quench the excited fluorophore (S_1 control) or extend its electronic delocalization (S_0 control) to allow the implementation of both photoactivation mechanisms reversibly.

2. EVOLUTION OF PHOTOACTIVATABLE FLUOROPHORES FROM MECHANISTIC PROBES TO BIOIMAGING TOOLS

The genesis of photoactivatable fluorophores can be traced back to the thorough spectroscopic studies of Lewis *et al.* on the photoisomerization of stilbene in 1940.²⁰ Their seminal contribution reported the appearance and growth of the characteristic fluorescence of *trans*-stilbene with its photochemical formation from *cis*-stilbene. Later, Förster proposed to monitor photochemical reactions with fluorescence measurements in order to probe the possible adiabatic formation of emissive products and provide insights on the potential energy surface of the excited state.²¹ Zweig eventually suggested the term photofluorescence to indicate the photochemical generation of fluorescent products and explored the use of "photofluorescent" compounds in high-speed photography.²²

The first biomedical application of fluorescence photoactivation was conceived, and experimentally demonstrated, almost four decades after the initial studies on the photoisomerization of stilbene.²⁰ Indeed, Sternson *et al.* reported a clinical assay for the analysis of the anti-cancer drug Tamoxifen, and one of its metabolites, in 1978.²³ It is based on the photoinduced conversion of both compounds into fluorescent products, the high-performance

liquid chromatographic separation of the photogenerated species and their quantitative determination with fluorescence detection. Incidentally, both molecules happen to be stilbene derivatives that convert into fluorescent phenanthrene analogues upon irradiation. In 1981, Angelides then demonstrated, with detailed spectroscopic studies, that a photoactivatable derivative of Tetrodotoxin is converted into a fluorescent product upon irradiation and that the photogenerated species binds covalently the receptor of this particular toxin.²⁴

Seminal imaging experiments, based on fluorescence photoactivation, followed shortly the early demonstration of photoaffinity labeling of toxin receptors. ²⁴ Specifically, Kraft *et al.* reported the first photocage—fluorophore construct (Figure 1) and suggested the term photoactivatable fluorophore, as well as the acronym PAF, for this general structural design in 1986. ²⁵ They further conceived an imaging strategy, called fluorescence photoactivation and dissipation (FPD), to monitor the diffusion of PAFs. The potential of fluorescence photoactivation to become an invaluable bioimaging tool was finally evident from the transformative experiments of Mitchinson. ²⁶ He demonstrated that FPD could track the dynamics of microtubules, labeled with a photocaged fluorescein, in live cells, stimulating the extension of this ingenious imaging strategy to the investigation of diverse dynamic processes in biological systems over the past three decades. In the wake of these studies, Haugland *et al.* also developed a variant of FPD, termed flow-tagging velocimetry, to monitor quantitatively flow dynamics in microstructured channels. ²⁷

Fluorescence photoactivation was later exploited, in conjunction with single-molecule detection, to overcome the stringent limitations that optical diffraction imposes on the spatial resolution of conventional fluorescence images. Indeed, Betzig *et al.* conceived a revolutionary imaging protocol, termed photoactivated localization microscopy (PALM), to enable the visualization of structural features in biological samples with nanometer resolution.²⁸ Their strategy evolved into a suite of imaging methods, all based on single-molecule detection with temporal differentiation, that are collectively called single-molecule localization microscopy (SMLM)²⁹ and are having transformative implications in biomedical research. Lippincott-Schwartz *et al.* further conceived

a variant of PALM for the high-throughput tracking of single-molecule dynamics in live cells, termed single-particle tracking PALM (spt-PALM)³⁰ with, once again, a significant impact on the fundamental understanding of cellular processes.

3. FLUORESCENCE PHOTOACTIVATION TO MONITOR DYNAMICS

Fluorescence recovery after photobleaching (FRAP) is generally the method of choice to monitor dynamic events with a fluorescence microscope.³¹ The convenience of this imaging protocol is predominantly a consequence of the fact that it relies on conventional fluorophores, which are, of course, readily available. A given sample is labeled with the fluorophores and a region of interest within the field of view is illuminated at an appropriate λ_{Ex} (a in Figure 2). If irradiation is performed with sufficient power density, for enough time and in the presence of an adequate concentration of molecular oxygen, the fluorophores in the illuminated area eventually bleach. After bleaching (b in Figure 2), the entire field of view is irradiated at λ_{Ex} to excite the intact fluorophores and detect fluorescence outside the bleached region of the sample (c in Figure 2). If the fluorophores can diffuse within the sample, however, fluorescence gradually recovers in the area that was originally bleached (d in Figure 2). As a result, the sequential acquisition of images allows the tracking of the translocating fluorophores in real time and the determination of their diffusion coefficient from the temporal evolution of the emission intensity in the bleached area. The high power densities and long irradiation times required for bleaching, however, can cause significant cytotoxicity and result in diffusion prior to the sequential image acquisition respectively. Additionally, fluorophores in anoxic samples may not bleach at all or require even harsher illumination conditions to undergo degradation. Furthermore, fluorescence turns off against a bright background with bleaching, limiting the accessible contrast levels in the subsequent images and complicating the long-term monitoring of diffusion.

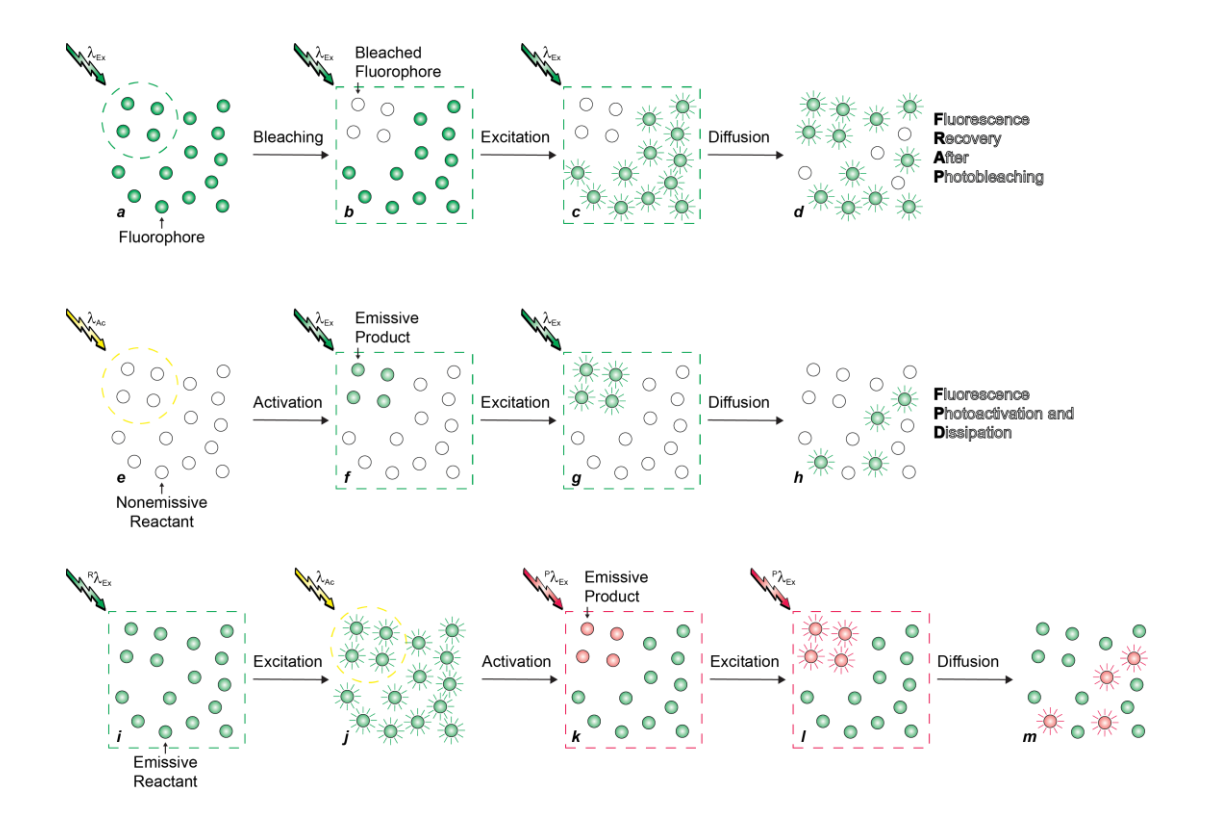


Figure 2. Sequences of steps required for the implementation of FRAP (a-d), FPD (e-h) and our imaging protocol (i-m) to monitor diffusion on the basis of the bleaching of selected fluorophores (FRAP), switching of their emission from off to on (FPD) and shifting the spectral region of their fluorescence (our protocol).

The stringent limitations inherent to the bleaching step, required for the implementation of FRAP, can be overcome with imaging schemes based on fluorescence photoactivation. Specifically, FPD relies on the photochemical conversion of PAFs from nonemissive to emissive states in a region of interest within a given sample under illumination at a suitable λ_{Ac} (e in Figure 2).²⁵ If the photochemical and photophysical properties of the PAFs are appropriately engineered, the illumination conditions sufficient for activation in FPD can be significantly milder than those necessary for bleaching in FRAP. Additionally, most PAFs can be activated efficiently even in the absence of molecular oxygen. After the activation step (f in Figure 2), the entire field of view can be illuminated at a suitable λ_{Ex} to detect fluorescence exclusively in the activated area (g in Figure 2). In analogy to FRAP, images collected sequentially then enable the tracking of the translocating

fluorophores in real time (*h* in Figure 2) and the determination of their diffusion coefficient from the temporal profile of the emission intensity measured in the activated area. In contrast to FRAP, however, fluorescence turns on against a dark background in FPD, facilitating signal detection and allowing the monitoring of the few photoactivated fluorescent species across the sample for long times. Nonetheless, the lack of any emission in the initial state of the PAFs prevents the acquisition of fluorescence images prior to activation. In turn, the inability to visualize the sample complicates the identification of regions within the field of view that would be appropriate for activation. In spite of these complications, photocaged acridinones, azafluorenones, benzothiazoles, borondipyrromethenes (BODIPYs), coumarins, cyanines, diazaxanthilidenes, fluoresceins, pyrazolines, resorufin, rhodamines, salens, tetraethylenes and xanthene have already been employed successfully to monitor diverse dynamic events in developing embryos and live cells on the basis of FPD.^{2–17}

We envisaged the possibility of overcoming the limitations of the original implementation of FPD with the realization of PAFs capable of interconverting between states with spectrally-resolved fluorescence, rather than switching from nonemissive to emissive species.³² Under these conditions, illumination of the sample at the excitation wavelength ($^{R}\lambda_{Ex}$) of the emissive reactant (i in Figure 2) and detection of its fluorescence in one spectral channel enables the visualization of the sample (i in Figure 2) and the identification of an optimal region of interest for activation. Irradiation of the selected area at λ_{Ac} converts the emissive reactants in the illuminated area into emissive products. Illumination of the entire field of view at the excitation wavelength ($^{P}\lambda_{Ex}$) of the product (i in Figure 2) and detection of its fluorescence in a separate detection channel (i in Figure 2) then allows the sequential acquisition of images to monitor the translocation of the photochemical products (i in Figure 2). As for the original version of FPD, their diffusion coefficient can be determined from the temporal evolution of their emission intensity in the activated area.

We developed a family of PAFs specifically designed for the implementation of our imaging protocol (*i-m* in Figure 2).^{32–39} They incorporate an *ortho*-nitrobenzyl (ONB) photocage⁴⁰ fused to an indole heterocycle through an oxazine ring (Figure 3). Upon irradiation at a λ_{Ac} within the main absorption band of the ONB group, the oxazine ring cleaves irreversibly to convert the [C-N] bond, fusing the two heterocycles of the reactant, into a [C=N] bond and release an orthonitrosobenzaldehyde. This structural transformation allows a given fluorescent chromophore, connected to the chiral center of the reactant (R² in Figure 3), to delocalize electrons over the adjacent indole heterocycle only in the product and, hence, shifts bathochromically its absorption and emission bands. Furthermore, the substituent (R¹ in Figure 3) in position 5 of the indole heterocycle can be manipulated with synthetic modifications to regulate the magnitude of the photoinduced bathochromic shift. Indeed, electronic delocalization from R¹ to R² can only occur in the photochemical product. As a result, the nature of R¹ has negligible influence on the spectral position of the absorption and emission bands of the reactant, but affects drastically those of the product. Furthermore, the intensity and position of the absorption band on the ONB group can be regulated with modifications of its substituent (R³ in Figure 3) to provide some level of control on the spectral range available for λ_{Ac} and dose of photons necessary for activation.

Figure 3. Structural design of our PAFs with substituents (R^1-R^3) available for the regulation of their photochemical and photophysical properties.

Compound 1 (Figure 4) is a representative example of our PAFs.³³ It incorporates a 4-methoxyphenylethynyl substituent at R¹ and a BODIPY fluorophore⁴¹ at R². Upon irradiation at a λ_{Ac} of 405 nm, the ONB group cleaves to generate 2 and bring R¹ and R² in electronic conjugation.³³ As a result, the absorption and emission bands of the BODIPY chromophore shift

bathochromically with the photoinduced conversion of 1 into 2 (a-d in Figure 4). The partiallyresolved fluorescence of reactant and product can be captured in separate detection channels of the same confocal laser-scanning microscope (CLSM) under excitation of 1 at a Rλ_{Ex} of 514 nm and of 2 at a Pλ_{Ex} of 633 nm. Specifically, 1 can be microinjected into developing *Drosophila* melanogaster embryos to stain the plasma membranes of the cellular blastoderm and allow their visualization in CLSM images captured under excitation at ${}^{R}\lambda_{Ex}$. After illumination of a portion of the blastoderm at λ_{Ac} , 1 switches to 2 exclusively in the irradiated area. CLSM images captured under excitation at P\(\lambda_{Ex}\) then permits the visualization of the few photoactivated cells and the subsequent diffusion of the photochemical products. Indeed, an overlap (e in Figure 4) of two images, recorded in the two detection channels immediately after activation, clearly shows the photochemical conversion in the activated area. Additionally, images (f-k in Figure 4), collected in the red channel sequentially after activation, reveal the gradual fluorescence redistribution across the focal plane. From the temporal evolution of the emission intensity in the activated area, the diffusion coefficient for the translocating molecules can be estimated to be $5.3 \times 10^{-8}~\text{cm}^2~\text{s}^{-1}$. Additional images, acquired after translating vertically the focal plane, demonstrate that the hydrophobic photochemical products can only diffuse horizontally within the hydrophobic platform of adjacent plasma membranes and cannot escape into the hydrophilic media above and below the cellular blastoderm.

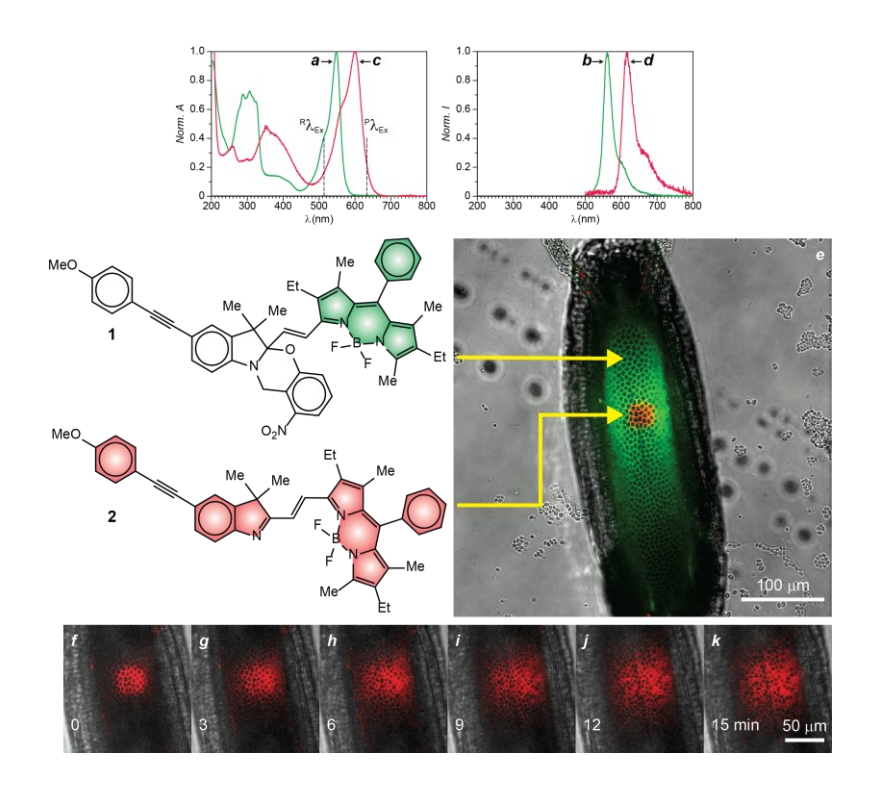


Figure 4. Normalized absorption and emission spectra of 1 (a and b) and 2 (c and d) in acetonitrile together with an overlap (e) of CLSM images, recorded in resolved spectral channels (green: $^{R}\lambda_{Ex}$ = 514 nm, $^{R}\lambda_{Em}$ = 525–600 nm; red: $^{P}\lambda_{Ex}$ = 633 nm, $^{P}\lambda_{Em}$ = 640–750 nm) after activation (λ_{Ac} = 405 nm, 50 mW cm⁻², 10 s) of the central region, of a *Drosophila melanogaster* embryo microinjected with 1 and images (f-k) captured sequentially in the red channel to monitor the gradual diffusion of 2.

The ability to change fluorescence color with activation allows the differentiation of emissive reactants from emissive products. $^{32-39}$ However, the activated species cannot be distinguished from each other. The differentiation of targets (*e.g.*, biomolecules, particles or even cells), labeled with the activated species, would require the photochemical transformation to generate, somehow, unique and stable fluorescence markers (barcodes) with spatial control. We satisfied this crucial requirement with the design of a PAF capable of switching among three states with spectrally-resolved fluorescence. Specifically, compound 3 (Figure 5) incorporates a BODIPY chromophores connected to two identical photocleavable oxazines. Upon irradiation at a λ_{Ac} of

405 nm, two consecutive photochemical reactions convert **3** through **4** into **5**. The photoinduced disconnection of the two ONB groups allows the central BODIPY chromophore to extend electronic delocalization over one and then both indole heterocycles. As a result, its absorption and emission bands shift bathochromically after each photoinduced step (*a*–*f* in Figure 5) to resolve sufficiently the fluorescence of the three compounds for their independent detection in three spectral channels of the same CLSM.

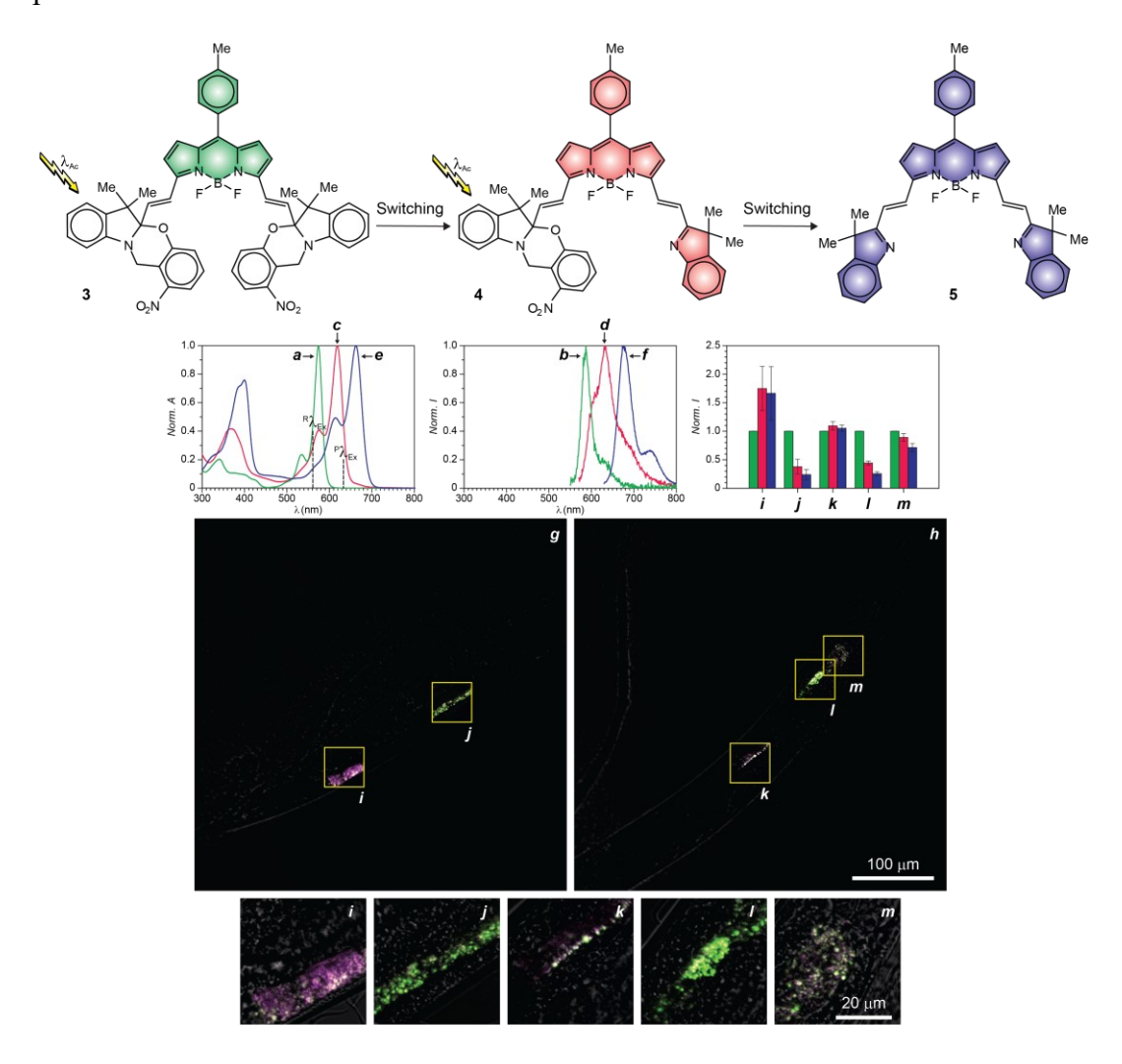


Figure 5. Normalized absorption and emission spectra of 3 (a and b), 4 (c and d) and 5 (e and f) in tetrahydrofuran together with overlaps of wide-field fluorescence images, recorded in resolved spectral channels (green: $^{R}\lambda_{Ex} = 561$ nm, $^{R}\lambda_{Em} = 575-600$ nm; red: $^{P}\lambda_{Ex} = 633$ nm, $^{P}\lambda_{Em} = 645-660$ nm blue: $^{P}\lambda_{Ex} = 633$ nm, $^{P}\lambda_{Em} = 750-800$ nm) after activation ($\lambda_{Ac} = 405$ nm, 50 mW cm⁻²)

along the intestinal tract of the tail (g) and head (h) regions of a *Caenorhabditis elegans* nematode, fed with polystyrene beads containing 3, for 5 (i), 0 (j), 10 (k), 0 (l) and 20 min (m) and the corresponding relative emission intensities (bar chart).

The relative amounts of the three interconverting compounds (3–5) and, hence, their relative emission intensities can be regulated precisely with adjustments in the dose of activating photons.³⁷ In turn, their photoregulated emission intensives can be detected in spectrally-resolved channels to provide the opportunity to "write" and "read" optical barcodes. For example, irradiation of selected regions (i-m in Figure 5) along the intestinal tract of the tail (g in Figure 5) and head (h in Figure 5) of a *Caenorhabditis elegans* nematode, fed with polystyrene beads containing 3, at a λ_{Ac} of 405 nm for different times allows the marking of each with a unique optical barcode. Indeed, the different dose of activating photons, incident on each of the five areas, converts different relative amounts of 3 into 4 and 5 to produce a unique set of relative emission intensities for each region of interest. Plots (bar chart in Figure 5) of the emission intensities detected for 5 and 4, relative to those measured for 3, show the barcodes corresponding to each activated area. Additionally, the polymer matrix around the fluorescent compounds protects the molecules form the surrounding environment. As a result, the barcodes are retained unaffected for extended periods of time, enabling the monitoring of the translocation of the photochemically barcoded polymer beads for hours within the intestinal tract of the live nematode.

Our protocol for optical barcoding and tracking of polymer beads in live organisms³⁷ may be especially valuable for spatially-resolved single-cell analysis over long timescales.⁴² For example, a large population of cells may be labeled with the initial emissive state of our three-color PAFs.³⁷ Selected cells may then be irradiated at λ_{Ac} for different times (\boldsymbol{a} in Figure 6) to generate in each different amounts of the three emissive compounds. Excitation of the three emissive species at the corresponding $^{R}\lambda_{Ex}$ and $^{P}\lambda_{Ex}$ (\boldsymbol{b} in Figure 6) may subsequently be exploited to capture images of the sample in three spectrally-resolved channels, quantify the relative emission intensities of the

three fluorescent compounds, determine the barcodes (c in Figure 6) of the few marked cells and track their dynamics for prolonged periods of time.

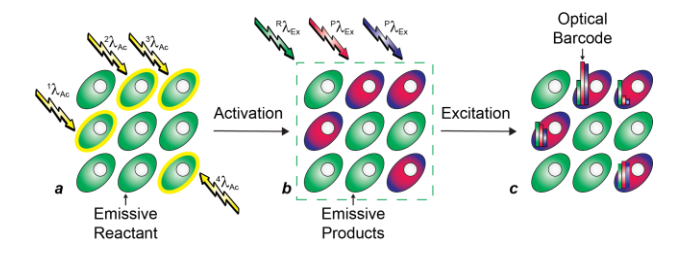


Figure 6. Sequence of steps (a-c) proposed for the photochemical barcoding and tracking of single cells on the basis of the photoinduced conversion of PAFs in selected cells under the influence of different doses of activating photons and the monitoring of their relative emission intensities.

4. FLUORESCENCE PHOTOACTIVATION TO OVERCOME DIFFRACTION

In a fluorescence microscope, exciting radiation travels from a laser source to the sample stage through an objective lens (*a* in Figure 7).⁴³ The excited emissive probes in the sample then produce fluorescence, which propagates through the very same objective lens to be detected on a camera. Specifically, the objective lens projects the collected fluorescence on the focal plane in the form of a diffraction pattern (Airy pattern), consisting of an inner disk (Airy disk) with concentric rings around it (*b* in Figure 7). The radius of the Airy disk is approximately half of the fluorescence wavelength, which generally happens to be in the visible region of the electromagnetic spectrum for most bioimaging applications. As a result, the Airy pattern spans across hundreds of nanometers on the focal plane, even when a single fluorophore with molecular dimensions produces fluorescence. In turn, the large dimensions of the diffraction pattern, relative to the size of molecules, limit the spatial resolution of conventional fluorescence images and prevent the visualization of structural features at the molecular level.

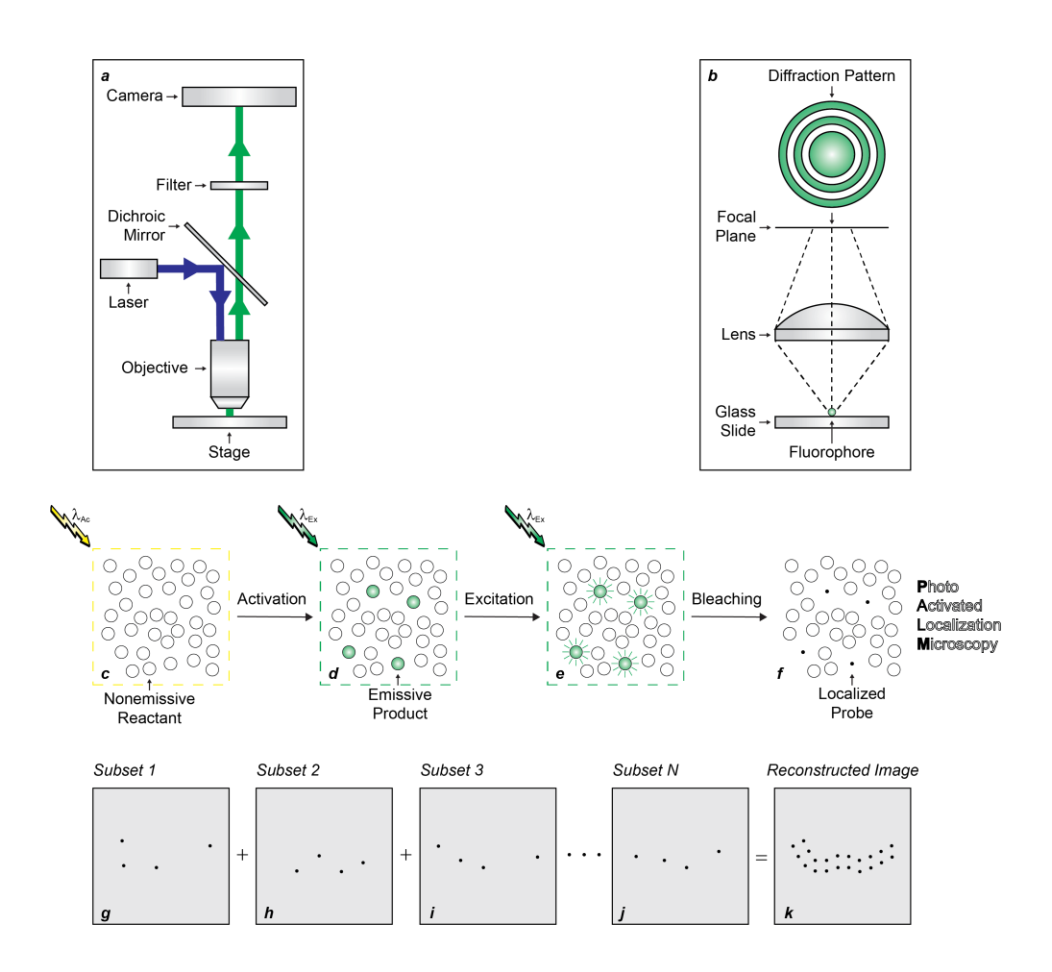


Figure 7. Schematic representations of a fluorescence microscope (a) and the diffraction pattern produced on the focal plane of the objective lens (b) together with the sequence of steps (c-k) required for the implementation of PALM on the basis of fluorescence activation and single-molecule localization.

PALM relies on fluorescence photoactivation to turn the emission of closely-spaced fluorophores on at different times and, in conjunction with single-molecule detection, differentiate temporally emissive species at subdiffraction separations.²⁸ Specifically, a given sample of interest is labeled with PAFs (c in Figure 7) and illuminated at λ_{Ac} with low power density to switch only a few of the many nonemissive reactants to the corresponding emissive products (d in Figure 7). These illumination conditions are essential to ensure negligible probability of finding two emissive species within the same diffraction area. If the emissive species are sufficiently bright for single-molecule detection, excitation of the sample at λ_{Ex} provides the opportunity to detect

concomitantly the diffraction patterns of the few spatially-resolved probes in the emissive state (e in Figure 7). If the emissive species can also undergo hundreds of excitation/emission cycles, the center of each diffraction pattern and, hence, the position of each fluorescent probe on the focal plane can be localized with precision at the nanometer level. Further excitation eventually bleaches the localized species, turning their fluorescence permanently off (f in Figure 7). A new subset of probes is then converted from nonemissive to emissive, localized with nanometer precision and bleached. The sequence of activation, localization and bleaching steps is reiterated thousands of times to provide the coordinates of a new subset of localized probes on the focal plane each time (g-j in Figure 7). The multiples subsets of coordinates are finally complied into a reconstructed image with subdiffraction resolution (k in Figure 7). Indeed, this ingenious protocol to overcome diffraction with PAFs has already been exploited successfully to visualize substructures of live cells with spatial resolution at the nanoscale. 12,13

The photochemical and photophysical properties of our PAFs (Figure 3) allow the reconstruction of subdiffraction images on the basis of PALM.³⁸ In particular, compound **6** (Figure 8) incorporates a styryl substituent on one of the two pyrrole heterocycles of the BODIPY fluorophore. The extended electronic delocalization of the chromophoric platform in this molecule shifts the BODIPY absorption and emission bands bathochromically and increases its molar absorption coefficient, relative to **1** and **3**. In spite of these noticeable changes in the BODIPY photophysics, the ONB photochemistry remains essentially unaffected. Upon irradiation at a λ_{Ac} of 405 nm, the ONB photocage cleaves to extend the electronic delocalization of the BODIPY fluorophore even further in **7**. Once again, the photoinduced structural transformation of reactant into product resolves partially their emission bands to enable the detection of their fluorescence in separate spectral channels. Additionally, the molar absorption coefficient ($\varepsilon = 73 \text{ mM}^{-1} \text{ cm}^{-1}$) and fluorescence quantum yield ($\phi = 0.41$) of **7** translate into appropriate brightness ($\varepsilon \times \phi = 30 \text{ mM}^{-1} \text{ cm}^{-1}$) for single-molecule detection. Indeed, the photoinduced conversion of a single molecule of **6** into **7** can be monitored within a rigid polymer matrix from the temporal fluorescence evolution

in the spectral region where the photochemical product emits. Under concomitant illumination of the sample at a λ_{Ac} of 405 nm and a $^{P}\lambda_{Ex}$ of 642 nm, the characteristic emission band of the photochemical product is detected after the photoactivation event (a in Figure 8). The photogenerated product then continues to undergo excitation/emission cycles for a few seconds before bleaching irreversibly. Thus, the single-molecule fluorescence of the photogenerated state of our PAF switches from off to on with activation and then from on to off with bleaching, enabling the implementation of the sequence of steps required for PALM.

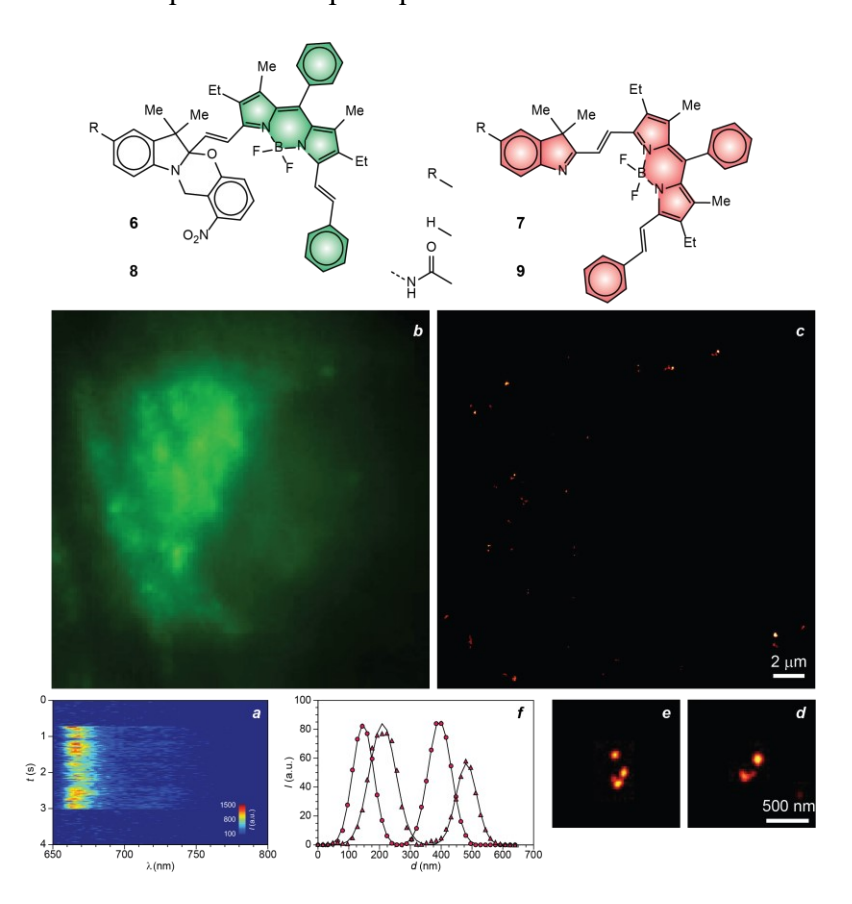


Figure 8. Evolution (*a*) of the single-molecule emission spectrum ($^{P}\lambda_{Ex} = 642 \text{ nm}$, 10 W cm⁻²) with the photoinduced conversion of 6 into 7 ($\lambda_{Ac} = 405 \text{ nm}$, 10 W cm⁻²) and bleaching of the latter compound in polymethyl methacrylate together with diffraction-limited (*b*: $^{R}\lambda_{Ex} = 532 \text{ nm}$, 10 W cm⁻²) and PALM (*c*: $\lambda_{Ac} = 405 \text{ nm}$, 10 W cm⁻²; $^{P}\lambda_{Ex} = 642 \text{ nm}$, 4 kW cm⁻²) images of COS-7 cells, labeled with 8, as well as magnifications (*d* and *e*) of the latter image with the

corresponding spatial distributions (f) of the emission intensities across the fluorescent organelles in the field of view.

The incorporation of an N-hydroxysuccinimide ester in position 5 of the indole heterocycle of 6 allows the nonselective covalent connection of the PAF to primary amino groups of intracellular proteins.³⁸ Indeed, incubation of this active ester with COS-7 cells results in intracellular bioconjugation and lysosomal localization. The characteristic fluorescence of the initial state of the bioconjugated PAF (8 in Figure 8) can clearly be observed in a diffraction-limited image (b in Figure 8) of a labeled cell captured with excitation at a ${}^{R}\lambda_{Ex}$ of 532 nm. The photochemical properties of the PAF are maintained after bioconjugation and illumination of the labeled cell at a λ_{Ac} 405 nm switches 8 to 9 with the expected bathochromic shift in fluorescence. In turn, irradiation at a Phas of 642 nm excites selectively the photochemical product to enable its singlemolecule localization with a precision of 15 nm in the interior of the live cell before bleaching it. As a result, sequences of activation, localization and bleaching steps permit the gradual identification of subsets of photoactivated probes and the reconstruction of a PALM image (c in Figure 8). Comparison of the diffraction-limited image (b in Figure 8), recorded before activation, and the subdiffraction image (c in Figure 8), compiled from 100,000 subsets of coordinates, of the very same cell reveals spatially-resolved nanostructures only in the latter. Magnifications (d and e in Figure 8) of the PALM image and profiles (f in Figure 8) of the emission intensity measured across two fluorescent nanostructures in each case indicate the visualized objects to have a diameter close to 80 nm, consistently with the physical dimensions expected for a lysosome. Thus, the unique combination of structural, photochemical and photophysical properties engineered into our PAF allow the visualization of subcellular features in live cells with a spatial resolution that would be impossible to achieve with conventional fluorescence imaging protocols.

The ability of PALM to overcome diffraction can also be exploited to monitor dynamic events at the single-molecule level.⁴⁴ Specifically, spt-PALM enables the sequential tracking of multiple subsets of single molecules with reiterative activation, excitation and bleaching steps analogous to

conventional PALM.³⁰ Once again, a sample labeled with PAFs is illuminated at an appropriate λ_{Ac} with low power density to convert only a sparse subsets of probes from their nonemissive to the emissive state (a in Figure 9). The few emissive products are then excited at their λ_{Ex} (b in Figure 9) and, if sufficiently bright, detected at the single-molecule level (c in Figure 9). If the fluorescent species are able to diffuse across the sample, the dynamics of each one of the activated PAFs can be monitored with sequential excitation/emission cycles until they bleach (d in Figure 9). A new subset of probes is then activated, tracked and bleached. The same sequence of events is reiterated multiple times to monitor each time the trajectories of a new subset of probes. The many subsets of trajectories (e-h in Figure 9) are finally compiled into a single map (i in Figure 9) to provide quantitative information on the dynamics of the tracked probes with statistical confidence. Indeed, spt-PALM and PAFs have already enabled the high-throughput tracking of single molecules in live cells.⁴⁵⁻⁴⁷

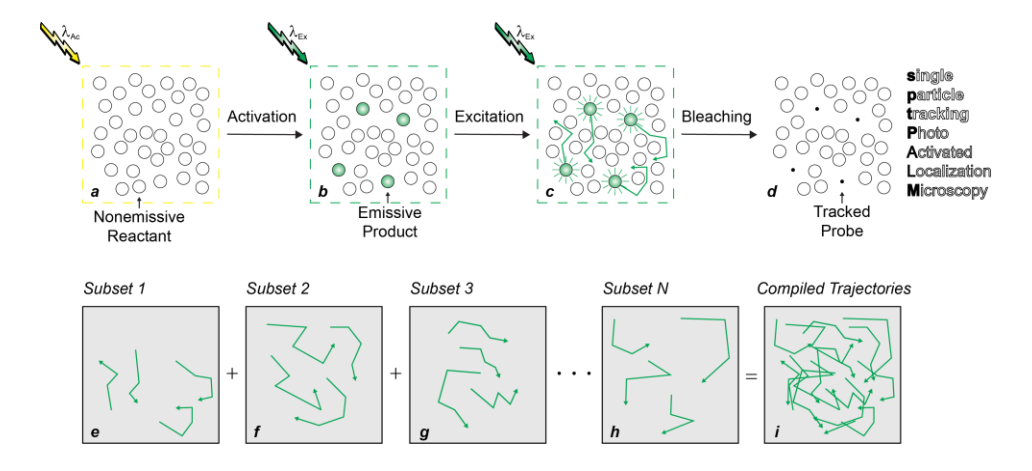


Figure 9. Sequence of steps (*a*–*i*) required for the implementation of spt-PALM on the basis of fluorescence activation and single-molecule tracking.

Our PAFs can also be tracked intracellularly at the single-molecule level on the basis of spt-PALM.³⁸ Illumination of COS-7 cells, labeled with 6 or 8, at a λ_{Ac} of 405 nm converts them to 7 or 9 respectively within the lysosomal compartments. Single molecules of the photochemical products can then be tracked over time under excitation at a ${}^{P}\lambda_{Ex}$ of 642 nm. The resulting images

show that 7 can move over ca. 350 nm in 40 ms (a–c and g in Figure 10), while 9 remains essentially in the same position over this timescale (d–g in Figure 10). Indeed, only the latter compound is covalently connected to intracellular proteins, which restrict its ability to translocate over this temporal scale.

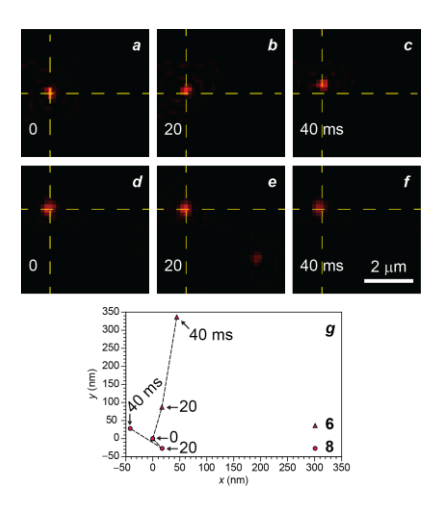


Figure 10. Single-molecule fluorescence images of COS-7 cells labeled with 6 (a–c) or 8 (d–f), recorded sequentially after activation ($\lambda_{Ac} = 405$ nm, 10 W cm⁻²; $^{P}\lambda_{Ex} = 642$ nm, 4 kW cm⁻²), and the single-molecule trajectories (g) of the corresponding photochemical products.

5. CONCLUSIONS

Countless synthetic dyes with absorption and emission bands in appropriate spectral regions for bioimaging applications are readily available from commercial sources. 48 Some of them even have sufficient brightness and adequate photon budgets for imaging schemes based on single-molecule detection. Commercial PAFs are, instead, limited to a few fluorescein derivatives with modest photochemical and photophysical properties. Some level of synthetic expertise is, therefore, generally required to access PAFs with optimal photochemical and photophysical parameters for the implementation of FPD, PALM and their variants. As a result, these promising imaging strategies still remain inaccessible to most biomedical laboratories. Experimental protocols to streamline the synthesis of large quantities of PAFs and allow their purification on a preparative

scale at the levels of purity required for single-molecule detection must be developed to enable the commercialization of these promising bioimaging probes.

Most of the present PAFs, including our own compounds (Figure 3), require ultraviolet radiation or violet light for photoactivation. 12,13 Many of the chromophores intrinsic to biological samples absorb in this spectral range. As a result, activation of PAFs in live specimens excites concomitantly some of the intrinsic chromophores to encourage possibly their photochemical degradation. Additionally, the photochemical reactions responsible for the activation of some PAFs involve the population of triplet states, which can promote the formation of singlet oxygen and, once again, the degradation of biological samples. Indeed, systematic cytotoxicity studies demonstrated that the illumination conditions commonly employed for fluorescence photoactivation cause significant cell mortality. Pegligible influence of irradiation on live cells was observed only at wavelengths longer than 500 nm with the typical power densities of fluorescence photoactivation. Nonetheless, only a few examples of fluorescence photoactivation with green or red light in live cells have been reported so far. One of the participation of triplet states, must be developed to avoid the detrimental effects that the short λ_{AC} of current PAFs have on biological samples.

The engineering of viable mechanisms to initiate photochemical reactions with red/green light is inherently challenging.⁵³ Additionally, the possible sensitivity of the resulting PAFs to ambient light may complicate their synthesis, purification and manipulation in the laboratory environment. Ideally, an intentional decrease in the activation quantum yield should accompany the bathochromic shift in λ_{Ac} to ensure negligible sensitivity to ambient light and allow activation only at power densities accessible with laser sources. An alternative approach to avoid the short λ_{Ac} of current PAFs and the complications associated with green/red-light activation may be to rely on two-photon absorption to initiate the photochemical reaction responsible for activation. Indeed, the activation of PAFs with the simultaneous absorption of two near-infrared photons has been

reported already.^{54–66} Nonetheless, two-photon absorption demands power densities in excess of 1 GW cm⁻², which are generally achieved with expensive and hazardous Ti:sapphire lasers capable of squeezing microjoules of energy into a single femtosecond pulse.⁶⁷ The technical challenges, towering costs and potential hazards associated with the operation of ultrahigh-power lasers may be avoided altogether relying on plasmonic effects to promote the simultaneous absorption of multiple photons under moderate illumination.⁶⁸ Indeed, we demonstrated already that the two-photon activation of PAFs can be achieved with relatively low power densities on the basis of plasmonic effects.^{69,70} However, the possible extension of these promising operating principles for fluorescence activation to bioimaging application still remains a challenging objective.

In addition to improving the photochemistry of the photocage/photochrome, future PAFs would also benefit from the optimization of the photophysics of the fluorophore. Applications based on single-molecule detection demand chromophores with large ε and high ϕ to ensure optimal brightness ($\varepsilon \times \phi$).²⁹ Additionally, the localization of single molecules can be achieved with nanometer precision only if several tens of emitted photons per individual chromophore are detected. Considering that unitary ϕ are hardly possible, not all the excitation events translate into emitted photons. As a result, a single molecule must tolerate hundreds of excitation/deactivation cycles without decomposing to provide a sufficient number of emitted photons for localization at the nanometer level. Additionally, some of the excitation events may be followed by intersystem crossing with the population of relatively long-lived triplet states. During the lifetime of the triplet state, the chromophore cannot contribute any emitted photons. It must return to the ground state, to be excited again, before being able to provide photons, delaying significantly the overall time required for localization. Furthermore, the participation of triples states may, once again, encourage the formation of singlet oxygen and the degradation of the sample. Thus, optimal structural designs for the fluorescent components of future PAFs must be identified to ensure appropriate brightness and photobleaching resistance together with negligible intersystem crossing.

AUTHOR INFORMATION

Corresponding Authors

Yang Zhang — Program of Polymer and Color Chemistry, Department of Textile Engineering, Chemistry and Science, North Carolina State University, Raleigh, NC 27606; Email: yang.zhang@ncsu.edu

Françisco M. Raymo — Laboratory for Molecular Photonics, Department of Chemistry, 1301 Memorial Drive, University of Miami, Coral Gables, FL 33146-0431; Email: fraymo@miami.edu

Notes

The authors declare no competing financial interest.

ACKNOWLEDGMENTS

The National Institutes of Health (NIGMS-R01GM143397 and R21GM141675) and National Science Foundation (CHE-1954430) are acknowledged for financial support.

REFERENCES

- 1 Lakowicz, J. R. *Principles of Fluorescence Spectroscopy*; Springer: New York, 2006.
- 2 Mitchison, T. J.; Sawin, K. E.; Theriot, J. A.; Gee, K.; Mallavarapu, A. Caged fluorescent probes. *Methods Enzymol.* **1998**, *291*, 63–78.
- Wysocki, L. M.; Lavis, L. D. Advances in the chemistry of small molecule fluorescent probes. *Curr. Opin. Chem. Biol.* **2011**, *15*, 752–759.

- 4 Puliti, D.; Warther, D.; Orange, C.; Specht, A.; Goeldner, M. Small photoactivatable molecules for controlled fluorescence activation. *Bioorg. Med. Chem.* **2011**, *19*, 1023–1029.
- 5 Raymo, F. M. Photoactivatable synthetic dyes for fluorescence imaging at the nanoscale. *J. Phys. Chem. Lett.* **2012**, *3*, 2379–2385.
- 6 Raymo, F. M. Photoactivatable fluorophores. ISRN Phys. Chem. 2012, 619251.
- Li, W.-H.; Zheng, G. Photoactivatable fluorophores and techniques for biological imaging applications. *Photochem. Photobiol. Sci.* **2012**, *11*, 460–471.
- 8 Raymo, F. M. Photoactivatable synthetic fluorophores. *Phys. Chem. Chem. Phys.* **2013**, *15*, 14840–14850.
- 9 Gorka, A. P.; Nani, R. R.; Schnermann, M. J. Cyanine polyene reactivity: scope and biomedical applications. *Org. Biomol. Chem.* **2015**, *13*, 7584–7598.
- Lavis, L. D. Teaching old dyes new tricks: biological probes built from fluoresceins and rhodamines. *Annu. Rev. Biochem.* **2017**, *86*, 825–843.
- 11 Chevalier, A.; Renard, P. Y.; Romieu, A. Azo-based fluorogenic probes for biosensing and bioimaging: recent advances and upcoming challenges. *Chem. Asian J.* **2017**, *12*, 2008–2028.
- Zhang, Y.; Raymo, F. M. Live-cell imaging at the nanoscale with bioconjugatable and photoactivatable fluorophores. *Bioconjugate Chem.* **2020**, *31*, 1052–1062.
- Zhang, Y.; Raymo, F. M. Photoactivatable fluorophores for single-molecule localization microscopy of live cells. *Methods Appl. Fluoresc.* **2020**, *8*, 032002.

- Zou, Z.; Luo, Z. L.; Xu, X.; Yang, S.; Qing, Z. H.; Liu, J. W.; Yang, R. Photoactivatable fluorescent probes for spatiotemporal-controlled biosensing and imaging. *Trends Anal. Chem.* 2020, 125, 115811.
- Ragab, S. S. Using organic compounds for fluorescence photoactivation. *Egypt. J. Chem.* **2021**, *64*, 2113–2126.
- Zhang, Y.; Zheng, Y.; Meana, Y.; Raymo, F. M. BODIPYs with photoactivatable fluorescence. Chem. Eur. J. 2021, 27, 11257–11267.
- 17 Kikuchi, K.; Adair, L. D.; Lin, J. R.; New, E. J.; Kaur, A. Photochemical mechanisms of fluorophores employed in single-molecule localization microscopy. *Angew. Chem. Int. Ed.* **2023**, *62*, e202204745.
- 18 Goeldner, M.; Givens, R. (Eds.) *Dynamic Studies in Biology: Phototriggers, Photoswitches and Caged Biomolecules;* Wiley-VCH: New York, 2005.
- 19 Irie, M.; Yokoyama, Y.; Seki, T. (Eds.) *New Frontiers in Photochromism;* Springer: New York, 2013.
- 20 Lewis, G. N.; Magel, T. T.; Lipkin, D. The absorption and re-emission of light by cis- and trans-stilbenes and the efficiency of their photochemical isomerization. J. Am. Chem. Soc. 1940, 62, 2973–2980.
- Förster, T. Diabatic and adiabatic processes in photochemistry. *Pure Appl. Chem.* **1970**, *24*, 443–449.
- Zweig, A. Photochemical generation of stable fluorescent compounds (photofluorescence). *Pure Appl. Chem.* **1973**, *33*, 389–410.

- Mendenhall, D. W.; Kobayashi, H.; Fongmei, L. S.; Sternson, L. A.; Higuchi, T.; Fabian, C. Clinical analysis of tamoxifen, an anti-neoplastic agent, in plasma. *Clin. Chem.* **1978**, *24*, 1518–1524.
- Angelides, K. J. Fluorescent and photoactivatable fluorescent derivatives of tetrodotoxin to probe the sodium-channel of excitable membranes. *Biochemistry* **1981**, *20*, 4107–4118.
- 25 Krafft, G. A.; Cummings, R. T.; Dizio, J. P.; Furukawa, R. H.; Brvenik, L. J.; Sutton, W. R.; War, B. R. Fluorescence photoactivation and dissipation (FPD). *Nucleocytoplasmic Transport*; Peters, R.; Trendelenburg, M. (Eds.), Springer-Verlag, Berlin, 1986, 35–52.
- 26 Mitchison, T. J. Poleward microtubule flux in the mitotic spindle: evidence from photoactivation of fluorescence. *J. Cell Biol.* **1989**, *109*, 637–652.
- 27 Lempert, W. R.; Magee, K.; Ronney, P.; Gee, K. R.; Haugland, R. P. Flow tagging velocimetry in incompressible flow using photo-activated nonintrusive tracking of molecular motion (PHANTOMM). *Exp. Fluids* **1995**, *18*, 249–257.
- Betzig, E.; Patterson, G. H.; Sougrat, R.; Lindwasser, O. W.; Olenych, S.; Bonifacino, J. S.; Davidson, M. W.; Lippincott-Schwartz, J.; Hess, H. F. Imaging intracellular fluorescent proteins at nanometer resolution. *Science* 2006, 313, 1642–1645.
- Sauer, M.; Heilemann, M. Single-molecule localization microscopy in eukaryotes. *Chem. Rev.* **2017**, *117*, 7478–7509.
- Manley, S.; Gillette, J. M.; Patterson, G. H.; Shroff, H.; Hess, H. F.; Betzig, E.; Lippincott-Schwartz, J. High-density mapping of single-molecule trajectories with photoactivated localization microscopy. *Nat. Methods* **2008**, *5*, 155–157.

- 31 Ishikawa-Ankerhold, H. C.; Ankerhold, R.; Drummen, G. P. C. Advanced fluorescence microscopy techniques — FRAP, FLIP, FLAP, FRET and FLIM. *Molecules* 2012, 17, 4047– 4132.
- Zhang, Y.; Swaminathan, S.; Tang, S.; Garcia-Amorós, J.; Boulina, M.; Captain, B.; Baker, J. D.; Raymo, F. M. Photoactivatable BODIPYs designed to monitor the dynamics of supramolecular nanocarriers. *J. Am. Chem. Soc.* 2015, 137, 4709–4719.
- 33 Zhang, Y.; Tang, S.; Sansalone, L.; Baker, J. D.; Raymo, F. M. A photoswitchable fluorophore for the real-time monitoring of dynamic events in living organisms. *Chem. Eur. J.* 2016, 22, 15027–15034.
- 34 Liu, X.; Zhang, Y.; Baker, J. D.; Raymo, F. M. A photoactivatable light tracer. *J. Mater. Chem. C* **2017**, *5*, 12714–12719.
- 35 Sansalone, L.; Tang, S.; Garcia-Amorós, J.; Zhang, Y.; Nonell, S.; Baker, J. D.; Captain, B.; Raymo, F. M. A photoactivatable far-red/near-infrared BODIPY to monitor cellular dynamics in vivo. ACS Sens. 2018, 3, 1347–1353.
- 36 Zhang, Y.; Tang, S.; Thapaliya, E. R.; Sansalone, L.; Raymo, F. M. Fluorescence activation with switchable oxazines. *Chem. Commun.* **2018**, *54*, 8799–8809.
- 37 Tang, S.; Zhang, Y.; Dhakal, P.; Ravelo, L.; Anderson, C. L.; Collins, K. M.; Raymo, F. M. Photochemical barcodes. *J. Am. Chem. Soc.* **2018**, *140*, 4485–4488.
- Zhang, Y.; Song, K. H.; Tang, S.; Ravelo, L.; Cusido, J.; Sun, C.; Zhang, H. F.; Raymo, F. M. Far-red photoactivatable BODIPYs for the super-resolution imaging of live cells. *J. Am. Chem. Soc.* 2018, 140, 12741–12745.

- 39 Thapaliya, E. R.; Mazza, M. M. A.; Cusido, J.; Baker, J. D.; Raymo, F. M. A synthetic strategy for the structural modification of photoactivatable BODIPY–oxazine dyads. *ChemPhotoChem* **2020**, *4*, 332–337.
- 40 Klán, P.; Šolomek, T.; Bochet, C. G.; Blanc, A.; Givens, R.; Rubina, M.; Popik, V.; Kostikov, A.; Wirz, J. Photoremovable protecting groups in chemistry and biology: reaction mechanisms and efficacy. *Chem. Rev.* 2013, 113, 119–191.
- 41 Loudet, A.; Burgess, K. BODIPY dyes and their derivatives: Syntheses and spectroscopic properties. *Chem. Rev.* **2007**, *107*, 4891–4932.
- 42 Kwok, S. J. J.; Martino, N.; Dannenberg, P. H.; Yun, S. H. Multiplexed laser particles for spatially resolved single-cell analysis. *Light Sci. Appl.* **2019**, *8*, 74.
- 43 Murphy, D. B. Fundamentals of Light Microscopy and Electronic Imaging; Wiley-Liss: New York, 2001.
- 44 Sengupta, P.; van Engelenburg, S. B.; Lippincott-Schwartz, J. Superresolution imaging of biological systems using photoactivated localization microscopy. *Chem. Rev.* 2014, 114, 3189–3202.
- 45 Grimm, J. B.; English, B. P.; Choi, H.; Muthusamy, A. K.; Mehl, B. P.; Dong, P.; Brown, T. A.; Lippincott-Schwartz, J.; Liu, Z.; Lionnet, T.; Lavis, L. D. Bright photoactivatable fluorophores for single-molecule imaging. *Nat. Methods* 2016, *13*, 985–988.
- 46 De Zitter, E.; Thedie, D.; Monkemoller, V.; Hugelier, S.; Beaudouin, J.; Adam, V.; Byrdin, M.; Van Meervelt, L.; Dedecker, P.; Bourgeois, D. Mechanistic investigation of mEos4b reveals a strategy to reduce track interruptions in sptPALM. *Nat. Methods* 2019, *16*, 707–710.

- 47 Cho, Y.; An, H. J.; Kim, T.; Lee, C.; Lee, N. K. Mechanism of cyanine5 to cyanine3 photoconversion and its application for high-density single-particle tracking in a living cell. *J. Am. Chem. Soc.* **2021**, *143*, 14125–14135.
- 48 Johnson, I. D. The Molecular Probes Handbook A Guide to Fluorescent Probes and Labeling Technologies; Life Technologies Corporation: Carlsbad, 2010.
- 49 Wäldchen, S.; Lehmann, J.; Klein, T.; van de Linde, S.; Sauer, M. Light-induced cell damage in live-cell super-resolution microscopy. *Sci. Rep.* **2015**, *5*, 15348.
- 50 Wijesooriya, C. S.; Peterson, J. A.; Shrestha, P.; Gehrmann, E. J.; Winter, A. H.; Smith, E. A. A photoactivatable BODIPY probe for localization-based super-resolution cellular imaging. Angew. Chem. Int. Ed. 2018, 57, 12685–12689.
- 51 Xu, Y.; Lin, S.; He, R.; Zhang, Y.; Gao, Q.; Ng, D. K. P.; Geng, J. C=C bond oxidative cleavage of BODIPY photocages by visible light. *Chem. Eur. J.* **2021**, *27*, 11268–11272.
- 52 Gong, Q.; Zhang, X.; Li, W.; Guo, X.; Wu, Q.; Yu, C.; Jiao, L.; Xiao, Y.; Hao, E. Long-wavelength photoconvertible dimeric BODIPYs for super-resolution single-molecule localization imaging in near-infrared emission. *J. Am. Chem. Soc.* **2022**, *144*, 21992–21999.
- 53 Turro, N. J.; Ramamurthy, V.; Scaiano, J. C. *Principles of Molecular Photochemistry*; University Science Books: Sausalito, 2009.
- 54 Kiskin, N. I.; Chillingworth, R.; McCray, J. A.; Piston, D.; Ogden, D. The efficiency of two-photon photolysis of a "caged" fluorophore, *o*-1-(2-nitrophenyl)ethylpyranine, in relation to photodamage of synaptic terminals. *Eur. Biophys. J.* **2002**, *30*, 588–604.

- 55 Majjigapu, J. R. R.; Kurchan, A. N.; Kottani, R.; Gustafson, T. P.; Kutateladze, A. G. Release and report: a new photolabile caging system with a two-photon fluorescence reporting function. *J. Am. Chem. Soc.* **2005**, *127*, 12458–12459.
- Dakin, K.; Li, W.-H. Infrared-LAMP: two-photon uncaging and imaging of gap junctional communication in three dimensions. *Nat. Methods* **2006**, *3*, 959.
- 57 Gagey, N.; Neveu, P.; Jullien, L. Two-photon uncaging with the efficient 3,5-dibromo-2,4-dihydroxycinnamic caging group. *Angew. Chem. Int. Ed.* **2007**, *46*, 2467–1469.
- 58 Fölling, J.; Belov, V. N.; Kunetsky, R.; Medda, R.; Schönle, A.; Egner, A.; Eggeling, C.; Bossi, M.; Hell, S. W. Photochromic rhodamines provide nanoscopy with optical sectioning. *Angew. Chem. Int. Ed.* **2007**, *46*, 6266–6270.
- Fölling, J.; Belov, V. N.; Riedel, D.; Schönle, A.; Egner, A.; Eggeling, C.; Bossi, M.; Hell, S.
 W. Fluorescence nanoscopy with optical sectioning by two-photon induced molecular switching using continuous-wave lasers. *ChemPhysChem* 2008, 9, 321–326.
- 60 Warther, D.; Bolze, F.; Léonard, J.; Gug, S.; Specht, A.; Puliti, D.; Sun, X.-H.; Kessler, P.; Lutz, Y.; Vonesch, J.-L.; Winsor, B.; Nicoud, J.-F.; Goeldner, M. Live-cell one- and two-photon uncaging of a far-red emitting acridinone fluorophore. *J. Am. Chem. Soc.* 2010, 132, 2585–2590.
- 61 Aquino, D.; Schönle, A.; Geisler, C.; Middendorf, C. v.; Wurn, C. A.; Okamura, Y.; Lang, T.; Hell, S. W.; Egner, A. Two-color nanoscopy of three-dimensional volumes by 4PI detection of stochastically-switched fluorophores. *Nat. Methods* 2011, 8, 353–359.
- 62 Jing, J.; Chen, J.-J.; Hai, Y.; Zhan, J.; Xu, P.; Zhang, J.-L. Rational design of ZnSalen as a single and two photon activatable fluorophore in living cells. *Chem. Sci.* **2012**, *3*, 3315–3320.

- Yu, Z.; Ohulchanskyy, T. Y.; An, P.; Prasad, P. N.; Lin, Q. Fluorogenic, two-photon-triggered photoclick chemistry in live mammalian cells. J. Am. Chem. Soc. 2013, 135, 16766–16769.
- 64 Zhou, L. Y.; Zhang, X. B.; Lv, Y. F.; Yang, C.; Lu, D. Q.; Wu, Y.; Chen, Z.; Liu, Q. L.; Tan, W. H. Localizable and photoactivatable fluorophore for spatiotemporal two-photon bioimaging. *Anal. Chem.* 2015, 87, 5626–5631.
- 65 Friedrich, F.; Klehs, K.; Fichte, A. H.; Junek, S.; Heilemann, M.; Heckel, A. A two-photon activatable amino acid linker for the induction of fluorescence. *Chem. Commun.* **2015**, *51*, 15382–15385.
- Mahmoodi, M. M.; Abate-Pella, D.; Pundsack, T. J.; Palsuledesai, C. C.; Goff, P. C.; Blank, D. A.; Distefano, M. D. Nitrodibenzofuran: a one- and two-photon sensitive protecting group that is superior to brominated hydroxycoumarin for thiol caging in peptides. *J. Am. Chem. Soc.* 2016, 138, 5848–5859.
- Bort, G.; Gallavardin, T.; Ogden, D.; Dalko, P. I. From one-photon to two-photon probes: "caged" compounds, actuators and photoswitches. *Angew. Chem. Int. Ed.* **2013**, *52*, 4526–4537.
- Abdulhalim, I. Coupling configurations between extended surface electromagnetic waves and localized surface plasmons for ultrahigh field enhancement. *Nanophotonics* **2018**, *7*, 1891–1916.
- 69 Garcia-Amoros, J.; Swaminathan, S.; Sortino, S.; Raymo, F. M. Plasmonic activation of a fluorescent carbazole-oxazine switch. *Chem. Eur. J.* **2014**, *20*, 10276–10284.

70 Impellizzeri, S.; Simoncelli, S.; Hodgson, G. K.; Lanterna, A. E.; McTiernan, C. D.; Raymo, F. M.; Aramendia, P. F.; Scaiano, J. C. Two-photon excitation of a plasmonic nanoswitch monitored by single-molecule fluorescence microscopy. *Chem. Eur. J.* 2016, 22, 7281–7287.

Graphical Abstract

